

## Structural transitions in $\text{Pb}(\text{In}_{1/2}\text{Nb}_{1/2})\text{O}_3$ under pressure

Muhtar Ahart<sup>\*,||</sup>, Maddury Somayazulu<sup>\*</sup>, Seiji Kojima<sup>†</sup>, Naohiko Yasuda<sup>‡</sup>,  
Sergey Prosandeev<sup>§,¶</sup> and Russell J. Hemley<sup>\*</sup>

<sup>\*</sup>*Geophysical Laboratory, Carnegie Institution of Washington  
5251 Broad Branch Rd., NW, Washington DC 20015, USA*

<sup>†</sup>*Institute of Materials Science, University of Tsukuba  
Tsukuba, Ibaraki 305-8573, Japan*

<sup>‡</sup>*Electrical and Electronic Engineering Department, Faculty of Engineering  
Gifu University, Gifu 501-1193, Japan*

<sup>§</sup>*Physics Department and Institute for Nanoscience  
and Engineering University of Arkansas  
Fayetteville, Arkansas 72701, USA*

<sup>¶</sup>*Department of Physics, Research Institute of Physics  
Southern Federal University, Rostov on Don 344090, Russia*

<sup>||</sup>maihaiti@carnegiescience.edu

Received 5 October 2015; Accepted 10 November 2015; Published 13 January 2016

Room-temperature Raman scattering and x-ray diffraction measurements together with first-principles calculations were employed to investigate the behavior of disordered  $\text{Pb}(\text{In}_{1/2}\text{Nb}_{1/2})\text{O}_3$  (PIN) under pressure up to 50 GPa. Raman spectra show broad bands but a peak near the  $380\text{ cm}^{-1}$  increases its intensity with pressure. The linewidth of the band at  $550\text{ cm}^{-1}$  also increases with pressure, while two of the Raman peaks merge above 6 GPa. Above 16 GPa, we observe additional splitting of the band at  $50\text{ cm}^{-1}$ . The pressure evolution of the diffraction patterns for PIN shows obvious Bragg peaks splitting above 16 GPa; consistent with a symmetry lowering transition. The transition at 0.5 GPa is identified as a pseudo-cubic to orthorhombic (*Pbam*) structural change whereas the transition at 16 GPa is isostructure and associated with changes in linear compressibility and octahedral tilting, and the transition at 30 GPa is associated to an orthorhombic to monoclinic change. First-principles calculations indicate that the *Pbam* structure is ground state with antiferrodistortion consistent with experiment.

**Keywords:** Relaxor ferroelectrics; high-pressure; structural phase transition.

### 1. Introduction

Lead-based perovskite relaxor ferroelectrics and related materials are being used in a new generation of electromechanical devices. They have high piezoelectric coefficients with electromechanical deformations that are one order of magnitude larger than those of conventional high piezoelectric  $\text{PbZrO}_3$ - $\text{PbTiO}_3$  (PZT) ceramics.<sup>1,2</sup> The exceptional electromechanical properties of these Pb-based materials have generated intense interest in both scientific and industrial communities. While extensive theoretical and experimental studies have advanced our understanding of relaxor ferroelectrics,<sup>3-9</sup> their properties are still poorly understood. These difficulties stem from the complexity of these materials, which have a high degree of compositional, structural, and polar disorder.

There are two groups of Pb-based relaxors, one is in which two mixed metal ions occupy B-site of perovskite structure with a molar ratio of 1/3 to 2/3, for example,  $\text{Pb}(\text{Mg}_{1/3}\text{Nb}_{2/3})\text{O}_3$  (PMN), and the other is in which two mixed metal ions occupy B-site of perovskite structure with a molar ratio of 1/2 to 1/2, for example  $\text{Pb}(\text{Sc}_{1/2}\text{Nb}_{1/2})\text{O}_3$  (PSN). Here we focus on the  $\text{Pb}(\text{B}'_{1/2}\text{B}''_{1/2})\text{O}_3$ -type relaxors, in particular on  $\text{Pb}(\text{In}_{1/2}\text{Nb}_{1/2})\text{O}_3$  (PIN), and the degree of cation ordering is known to depend on the heat treatment procedure adopted at high temperature. For example, a well-annealed samples of B-site ordered PSN,<sup>10</sup>  $\text{Pb}(\text{Sc}_{1/2}\text{Ta}_{1/2})\text{O}_3$  (PST),<sup>11</sup> and PIN<sup>12</sup> undergoes a normal ferroelectric/antiferroelectric phase transition, while a quenched one with a B-site disordered  $\text{Pb}(\text{B}'_{1/2}\text{B}''_{1/2})\text{O}_3$  shows relaxor properties.

Three different PIN crystals, the ordered PIN, the disordered PIN, and the partly disordered PIN, are obtained by

different thermal treatments and which has different chemical ordering in the arrangement of  $\text{In}^{3+}$  and  $\text{Nb}^{5+}$  on the B-site,<sup>12–16</sup> respectively. It was reported that the ordered PIN shows a first-order phase transition from a paraelectric phase ( $Fm\text{-}3m$ ,  $Z = 8$ ) to an antiferroelectric phase ( $Pbam$ ,  $Z = 8$ ) at about  $160^\circ\text{C}$ , the disordered PIN shows the relaxor behavior characterized by a dielectric dispersion below  $50^\circ\text{C}$ ;<sup>17,18</sup> and the partly disordered PIN shows a broad peak of dielectric constant without dielectric dispersion around  $90^\circ\text{C}$ .<sup>16</sup> It should be noted that the ordered PIN undergoes an antiferroelectric transition with lowering of temperature, and in contrast to both ordered PSN<sup>17,18</sup> and PST<sup>19</sup> which undergo ferroelectric transitions.

Application of pressure can tune the physical properties, introduce new phenomena,<sup>7–9</sup> suppresses the diffuse scattering, and induce structural change in relaxor materials.<sup>20–25</sup> For example, disordered PIN undergoes a structural phase transition under pressure from a pseudo-cubic to an orthorhombic at 0.5 GPa.<sup>15,26</sup> Furthermore, pressure can help to resolve the structural complexities of relaxors because external elastic forces can slow down dynamic structural fluctuations and thus reveal the intrinsic structural features better. Reference 26 reported high-pressure Raman scattering and X-ray diffraction indicating that disordered PIN undergoes successive transitions under pressure. Here, we use high-pressure Raman scattering, X-ray diffraction, and first-principle calculations to systematically study the pressure dependence of diffuse scattering, the pressure-induced structural transitions, and the mechanism of these transitions in disordered PIN at room temperature.

## 2. Methods

Single crystal samples of the PIN were prepared by solid-state reaction according to the process described in Ref. 12. A crystal with dimensions of  $70 \times 70 \times 20 \mu\text{m}^3$  was obtained from a mm-sized grown single crystals and orientated with the largest faces parallel to  $(001)_{\text{cub}}$ . This was loaded into a diamond anvil cell (DAC) with neon as the pressure medium for single crystal diffraction. A chip of ruby was also loaded for pressure determination. Small amounts of powder samples (crushed from single crystal) of PIN were loaded into separate DACs with argon as the pressure medium for X-ray powder diffraction and Raman scattering experiments.

The X-ray diffraction experiments were carried out at beamline 16-ID-B of HPCAT at the Advanced Photon Source, Argonne National Laboratory. In this experiment, a pre-monochromator combined with a  $\text{Si}(311)$  crystal was employed to provide the monochromatic incident beam with a wavelength close to  $0.4 \text{ \AA}$ . A MAR3450 image plate was used to record oscillation photographs for powder diffraction and a MARCCD was used for single crystal diffraction. The standard ruby luminescence technique was used to determine the pressure, with an estimated accuracy of 0.2 GPa. Additional experimental details about the beamline can be found

in Ref. 27; further information on the Raman scattering setup as well as the procedures can be found in Refs. 24 and 28.

We also performed first-principles calculations using used PBE pseudopotentials<sup>29</sup> as implemented in the VASP package.<sup>30</sup> Electron wave functions were truncated at 500 eV. We considered several different unit cells with different geometries in order to find the ground state and calculate the relative enthalpies at 0 K.

## 3. Results

### 3.1. Raman spectroscopy

Figure 1 shows a set of representative Raman spectra of PIN at selected pressures. The bands are broad in comparison to the first-order scattering of conventional ferroelectrics, such as  $\text{PbTiO}_3$ , which show sharp peaks in their polar phases. Because of their inherent complexity the measured spectra of relaxor are consisted with the phonon densities of states as well as excitations with intensities determined by frequency dependent Raman matrix elements. However, reasonable results could be achieved by careful examination of the pressure dependences of fits to the spectra. Our results are presented to reflect general trends observed in this class of materials under pressure (Fig. 2). It should be noted that the low frequency modes centered around  $50 \text{ cm}^{-1}$  show a slight pressure dependence, hardening on compression up to 16 GPa and consistent with previous measurements on several other lead-based relaxors.<sup>22,24</sup> Interestingly, this mode displays obvious splitting above 16 GPa, as shown in inset of Fig. 2(b), indicating a possible symmetry lowering phase transition. Five other regions in Raman spectra also show interesting changes under pressure. The first is a peak around  $130 \text{ cm}^{-1}$  that appears as a shoulder of the main low frequency peak above 0.5 GPa (Fig. 3). This peak is associated with the transition that occurs at 0.5 GPa and confirm the

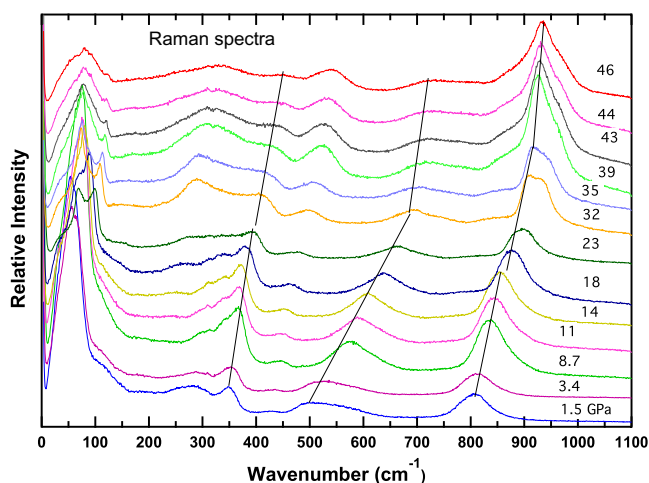


Fig. 1. Selected high-pressure Raman spectra of PIN. Solid lines show the pressure evolutions trend of main Raman bands.

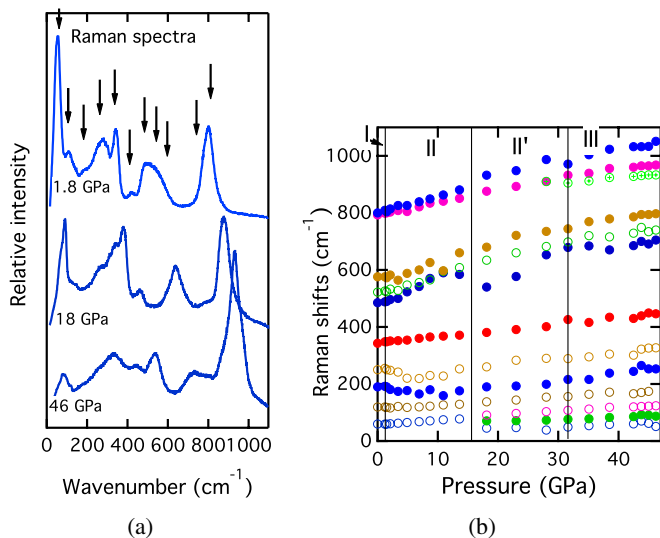


Fig. 2. High-pressure Raman spectra of PIN. (a) Spectra at 1.8 GPa, 18 GPa, and 46 GPa and (b) pressure dependencies of the observed Raman features. The vertical lines indicate the approximate phase boundaries.

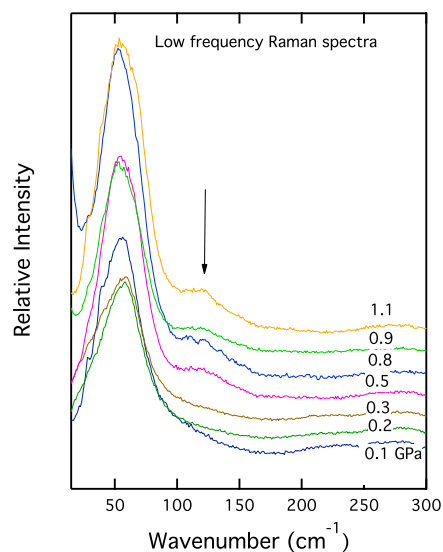


Fig. 3. Low-frequency Raman modes at selected pressures. Arrow shows appearance of a peak around  $130\text{ cm}^{-1}$  above 0.5 GPa and indicative of the first structural transition.

observation by Nomura *et al.* using X-ray diffraction.<sup>12</sup> The next one is a sharp peak near  $380\text{ cm}^{-1}$  that increases in intensity with increasing pressure. The third is a broad band around  $550\text{ cm}^{-1}$  which we decompose into three peaks with two broad peaks merge together around 16 GPa. The fourth region is centered around  $800\text{ cm}^{-1}$ , which show obvious splitting above 16 GPa. Finally, we note that the entire Raman spectrum shows drastic change above 30 GPa.

Previous studies of the pressure and temperature dependence of Raman spectra of relaxor materials have used PMN

as a model system for interpretation. For example, PMN, an end member of PMN- $x$ PT solid solutions, has a cubic perovskite structure. It has a Raman spectrum similar to that of the other compositions. The strong Raman scattering observed in PMN has been attributed to local chemically ordered regions. Experimental evidence for the presence of locally ordered regions has been obtained from transmission electron microscopy (TEM) which indicates chemical short-range order.<sup>31</sup> Specifically, 1:1 ordered domains of  $50\text{ \AA}$  in size are formed in these relaxors.<sup>31</sup> These ordered clusters in PMN reflected a cubic  $Fm\text{-}3m$  symmetry with the normal mode decomposition of  $2F_{2g}+E_g+A_{1g}$ , which is consistent with rocksalt-type ordering. Despite that our samples show orthorhombic structures at modest pressure, the Raman bands display similar features as that of the PMN samples. Although, there exists high pressure Raman scattering measurements on the relaxor materials such as PSN<sup>25,32</sup> and PST,<sup>33</sup> they are more closer to our sample PIN in terms of two metal cations occupy B-site of perovskite in a half and half mole ratio. The Raman spectra of pseudo-cubic PIN sample (at room temperature and ambient pressure) are also similar to that of PSN<sup>32</sup> or PST<sup>33</sup> contrary to the structural difference, i.e., PSN and PST have ferroelectric state ( $R3m$ ) at room temperature and ambient pressure. But considering PMN is a prototype example, and can be used as a model system to explain many features of relaxor materials with the perovskite structure; we will use this simplified model (PMN system),  $2F_{2g}+E_g+A_{1g}$ , to explain observed Raman spectra up to 16 GPa.

Within the frame of this model, the  $A_{1g}$  band at  $800\text{ cm}^{-1}$  results from the mode of fully symmetrical breathing vibration of oxygen octahedra. As shown in Fig. 2, this mode slightly hardens with pressure, while its linewidth is insensitive to pressure up to 16 GPa. The  $E_g$  band at  $550\text{ cm}^{-1}$  corresponds to the antiphase breathing mode of oxygen octahedra. This mode is degenerate and splits into two or more modes with a lower symmetry distortion. However, the remaining complex Raman features are the evidences for a lowering of symmetry from the  $Fm\text{-}3m$  selection rules. We should note one important point in relaxors, the polar and chemical disorder cause vibration modes to have coherence lengths that are small compared with their wavelengths. Such modes are not characterized by a single wave vector and will not obey momentum selection rules; all wave vectors contribute to the scattering process, causing broad features.<sup>34</sup> Thus direct use of group theory to assign all Raman modes based on the crystal symmetry is problematic.

One of the interesting results is our observation of the splitting of the Raman band at  $50\text{ cm}^{-1}$ , which is not observed for other Pb-based relaxor materials, for example, PMN,<sup>7</sup> or PMN- $x$ PT,<sup>7,35</sup> or PZN- $x$ PT.<sup>24</sup> Pressure suppresses the local polar distortions in many relaxor ferroelectrics. In addition, pressure enhances the tilting and can be seen in peak splitting and observed antiferroelectric state in PIN at modest pressure.

### 3.2. Single crystal X-ray diffraction

A PIN crystal was contained in a diamond anvil high-pressure cell (DAC) with a large opening angle ( $70^\circ$ ). Neon was used as the pressure-transmitting medium and single-crystal diffraction intensity measurements of PIN crystals up to 22 GPa were performed with an area detector (MarCCD) at 16-IDB, HPCAT of APS, Argonne National Laboratory. Data collection and analysis were done based on the technique and software developed by Dera *et al.*<sup>36</sup> The unit cell parameters were determined by least-squares refinement using the peak positions of 77 reflections indexed to an orthorhombic cell.

Figure 4 shows a typical single crystal diffraction image. An orthorhombic unit cell was used for indexing each Bragg peak. Refined lattice constants were  $a = 5.78 \text{ \AA}$ ,  $b = 11.2 \text{ \AA}$ ,  $c = 8.2 \text{ \AA}$ , with the space group of  $Pbam$  at 1.2 GPa. The diffuse scattering peaks were neglected during structure refinement; for example, at the lower part of the diffraction image (Fig. 5), there exist two strong wings around Bragg peak of  $[-16-2]$ . The same orthorhombic structure persists up to 22 GPa. It should be noted the refinements of atomic positions and its thermal parameters had practical problems because of the existence of strong diffuse scattering around Bragg peaks, and therefore refinements were limited to lattice parameters and determining space groups.

The butterfly-shaped diffuse scattering is the common feature of relaxor ferroelectrics. It has been observed in all

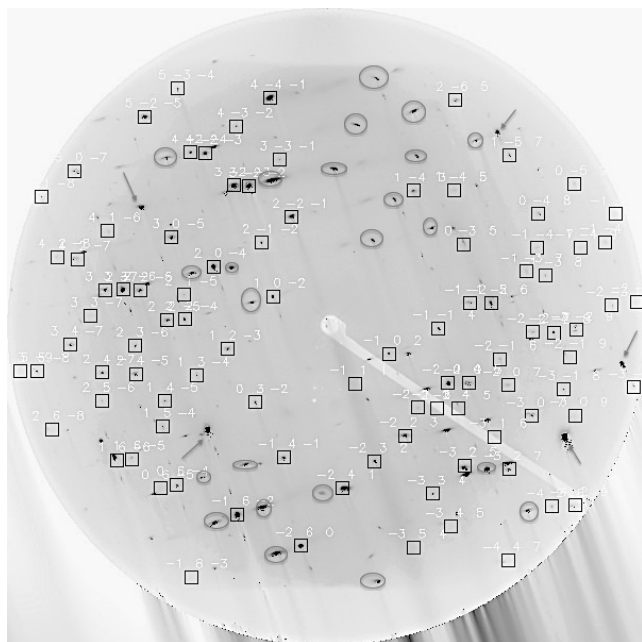


Fig. 4. Single crystal diffraction pattern at 1.2 GPa. An orthorhombic unit cell is used for indexing each Bragg peak. Refined lattice constants are:  $a = 5.78 \text{ \AA}$ ,  $b = 8.2 \text{ \AA}$ ,  $c = 11.2 \text{ \AA}$ , with the space group of  $Pbam$ . Each Bragg peak was boxed by a square; arrows indicate the Bragg peaks originated from diamond anvils and circles indicate the main diffuse streaks. Note the diffuse scattering peaks are neglected during structure analysis.

Pb-based relaxor materials such as PMN,<sup>21</sup> PZN-PT,<sup>24</sup> PSN,<sup>37</sup> etc. We also observed diffuse scattering in disordered PIN. For example, we showed butterfly-shaped diffuse scattering around  $(-1, 6, -2)$  Bragg peak in Fig. 5(c). In addition, we also observed diffuse scattering along the primary, lattice zones as seen in Fig. 5(a). The diffuse scattering along the lattice zones was reported in classic ferroelectric materials such as  $\text{BaTiO}_3$  (BTO) by Comes *et al.*<sup>38</sup> (reported in early 1970s). Consequently, Comes *et al.*, proposed the 8-site model to explain the transitions in BTO. It states that in cubic phase of BTO there are 8-equivalent-sites for Ti atom to occupy, these in turn generate diffuse scattering along the lattice zones; on lowering temperature, BTO undergoes a cubic to tetragonal transition. The Ti-atom continues to occupy a 4-fold degenerate site and still generate diffuse scattering along the lattice zones. This is followed by an orthorhombic phase in which BTO exhibits diffuse scattering with a 2-fold symmetry and eventually no diffuse scattering in the rhombohedral phase.

By comparing the form of the diffuse scattering streaks between BTO and PIN, we find that in PIN, the diffuse scattering is more complex than that reported in BTO. However, pressure suppresses diffuse scattering in both the materials. In Figs. 5(e) and 5(f), we plotted the pressure dependencies of integrated intensity and correlation size for the butterfly shaped diffuse scattering (we first convert the one wing (upper right wing in Fig. 5(c)) of butterfly shaped diffuse scattering from 2D image into an intensity profile at each pressure and the spectra are shown in Fig. 5(e)). Then we fit each spectrum by a Lorentzian function, which provides the integrated intensity and line width of each peak). Correlation size is therefore proportional to the inverse of half-line width. Both of them decrease with pressure and our observation is hence consistent with previous studies.<sup>21,24,37</sup>

### 3.3. Powder diffraction

Powder diffraction data were collected directly from the powder samples within the DAC using an area (Mar3450) detector. The samples were oscillated from  $-6^\circ$  to  $6^\circ$  in omega to improve powder averaging. The pressure dependence of the diffraction patterns was measured between ambient pressure and 50 GPa, and selected spectra were shown in Fig. 6(top panel). Figure 6(middle panel) shows the pressure-dependent pseudo-cubic (111)pc and (210)pc Bragg peaks.

A major change in the spectrum occurs around 30 GPa, when the structure transforms from orthorhombic to monoclinic, as indicated by the appearance of the triplet at  $2\theta = 12^\circ$ . Spectral changes also occurred at above 16 GPa, but the changes are possible due to the different linear compressibilities along the three axes. The presence of similar features in the spectra between 30 and 50 GPa indicates that no major structural change takes place in the high-pressure region.

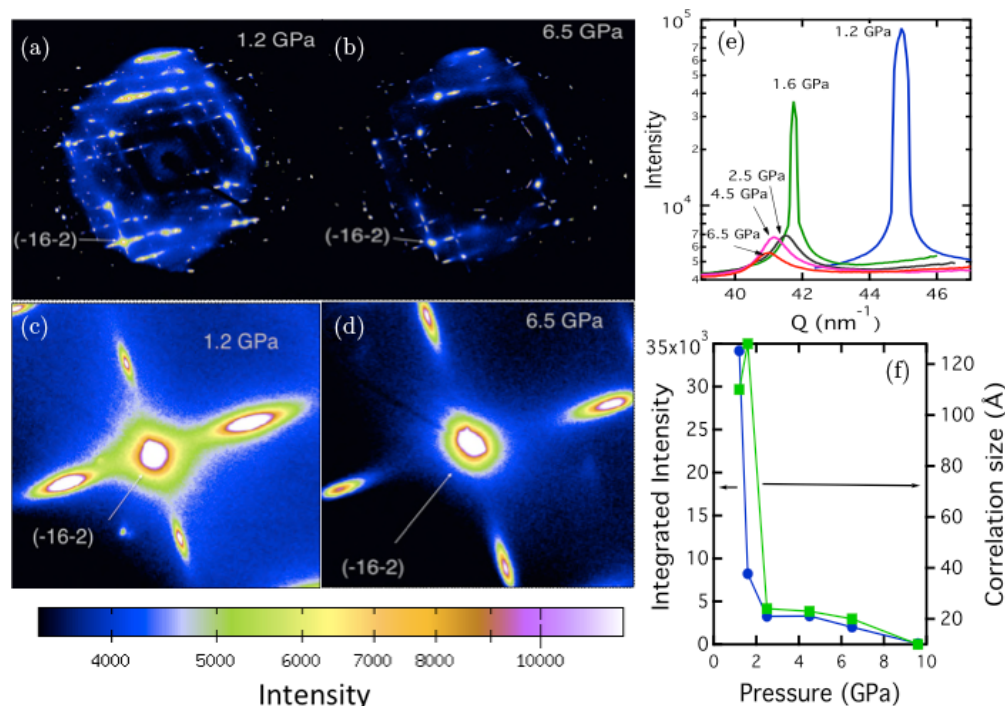


Fig. 5. Diffuse scatterings in PIN crystal. (a) Diffraction image including diffuse scatterings at 1.2 GPa. (b) Diffraction image including diffuse scatterings at 6.5 GPa. (c) Butterfly-shaped diffuse scattering around  $(-16-2)$  Bragg peak at 1.2 GPa. (d) Butterfly-shaped diffuse scattering around  $(-16-2)$  Bragg peak at 6.5 GPa. (e) Intensity profile for diffuse scattering (from one wing: upper right wing in of butterfly-shaped diffuse scattering at selected pressures. (f) Pressure dependencies of integrated intensity (solid circles) and correlation size (solid squares) of butterfly-shaped diffuse scattering.

We carried out the least-squares fitting for the diffraction data (GSAS<sup>39</sup>) obtained below 30 GPa; above 30 GPa, using diffraction peak positions via Dicol-program calculated monoclinic lattice parameters, the  $\beta$ -angle, and volumes. As an example, Fig. 6(bottom panel) shows Rietveld fitting results for the spectrum at 3.9 GPa. In the figure, the dots are experimental data, solid curves are fitted results, and residual is shown as well. The pressure dependencies of the lattice parameters ( $a$ ,  $b$ ,  $c$ ), and the unit cell volume are plotted in Fig. 7 and numerical values (including the  $\beta$ -angle) are tabulated in Table 1. Rietveld fitting parameters such as atomic positions at 3.9 and 24 GPa are shown in Table 2. Lattice parameters  $a$ ,  $b$  and  $c$  behave normally (Fig. 7), i.e., they all decrease smoothly with pressure up to 50 GPa, however, the linear compressibilities are different for each of them. Figure 7 shows that the unit cell volumes of all phases vary smoothly with pressure and the volume changes at the transitions seem to be small. However, the normalized pressure,<sup>40</sup>

$$\left(\frac{P}{\{3f(1+2f)^{5/2}\}}\right), \quad (1)$$

where  $P$  is pressure and  $f$  is Euler strain, as the function of Euler strain,

$$(f = \{(V_0/V)^{2/3} - 1\}/2), \quad (2)$$

where  $V_0$  is initial volume and  $V$  is volume at  $P$ , shows changes around 16 and 33 GPa indicative of the transitions

(inset of Fig. 7(d)). A third-order Birch–Murnaghan equation of state (EOS)

$$P = (3K_0/2)[(V_0/V)^{7/3} - (V_0/V)^{5/3}] \{1 + 3/4(K'_0 - 4)[(V_0/V)^{2/3} - 1]\}, \quad (3)$$

where  $K_0$  is bulk modulus and  $K'_0$  is its pressure derivative, is applied to fit the pressure dependence of unit cell volume, which yields a bulk modulus of  $99 (\pm 16)$  GPa, its pressure derivative of  $8 (\pm 2)$ , and an initial volume of  $560 (\pm 3) \text{ \AA}^3$  below 33 GPa; a separated fit to the data above 33 GPa yields a bulk modulus of  $316 (\pm 20)$  GPa, its pressure derivative of 4 (fixed), and an initial volume of  $521 (\pm 15) \text{ \AA}^3$ . Figure 8 shows a structure model (orthorhombic  $Pbam$ ) constructed from the parameters obtained from a Rietveld fitting at 3.9 GPa. The structural model indicates the Pb displacements in the  $\Sigma$ -mode (antiferroelectric displacements), and oxygen-octahedra rotations in the  $R$ -mode in Brillouin zone are co-existing. These results are consistent with the highly compacted nature in the perovskite structure with  $\text{In}_{1/2}^{+3} + \text{Nb}_{1/2}^{+5}$  and  $\text{Pb}^{+2}$  cations being 6- and 12-coordinated, respectively. The subtle changes between the high-pressure polymorphs are in part due to the tilt and/or the rotation of the  $\text{In}_{1/2}\text{Nb}_{1/2}\text{O}_6$  octahedrons and in part due to the distortion of the octahedral ( $\text{In}_{1/2}\text{Nb}_{1/2}\text{O}_6$ ) and dodecahedral ( $\text{PbO}_{12}$ ) sites. The fundamental units

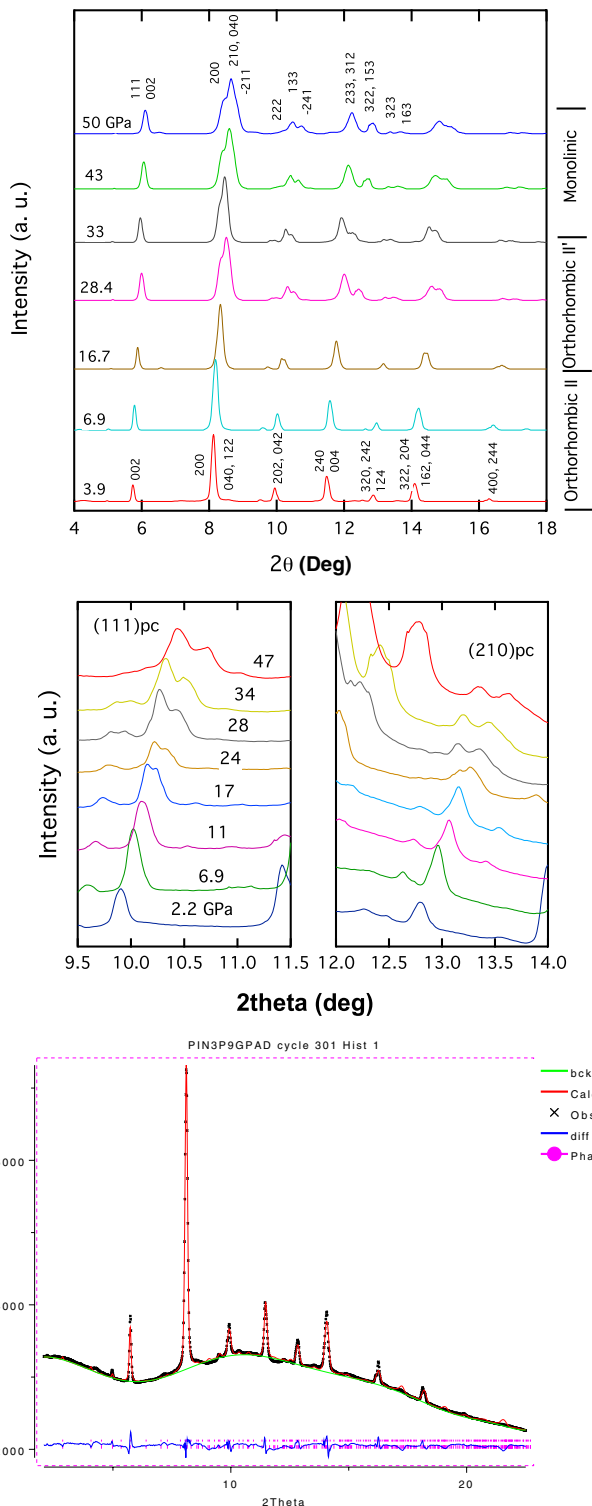


Fig. 6. Powder diffraction patterns. (Top panel) Diffraction patterns at selected pressures. Orthorhombic  $Pbam$  Indexing was used below 33 GPa, and monoclinic indexing was used above 33 GPa. (Middle panel) Pressure dependencies of the pseudo-cubic  $(110)_{pc}$  and  $(210)_{pc}$  Bragg peaks. (Bottom panel) A typical example of Rietveld refinement fitting at 3.9 GPa.  $R_p = 0.0099$  and  $wR_p = 0.0144$ .

such as the octahedral  $In_{1/2}Nb_{1/2}O_6$  and dodecahedral  $PbO_{12}$  in the PIN structure are therefore believed to be preserved all the way to 50 GPa. The pressure evolution of X-ray diffraction pattern in PIN samples is consistent with the results deduced from Raman scattering.

### 3.4. Theoretical calculations

To understand the atomistic mechanism of phase transitions in PIN under pressure, we performed first-principles calculations. We considered several different structures with different geometries up to 10 GPa. We started from the  $BaZrO_3$  (BZO) geometry given by  $Pbam$  space group symmetry, and then supplemented this structure with  $R3c$  and  $Pnma$ , for the sake of comparison. After that, these configurations were relaxed from the initial atomic displacements provided by BZO geometry, but already with the In and Nb ions substituting the Zr ions and Pb substituting Ba, in the NaCl structure. In the result, the  $R3c$  symmetry is lowered to  $R3$ , while both  $Pbam$  and  $Pnma$  convert to the monoclinic space group  $P2_1/c$ . The latter fact is of interest because the different ions in the B-positions produces the monoclinic distortion automatically. The strength of this monoclinic deformation can be different at different pressures. Our simulations show that the monoclinic distortion increases at high pressure.

The dependencies of the relative volumes on pressure of these phases are given in Fig. 9(a). We show here the starting symmetries of BZO, in order to distinguish between the two different  $P2_1/c$  structures. One can see that  $Pbam$  phase has the largest volume, followed by  $R3c$  and  $Pnma$ . Other phases in between are possible owing to different twin's configurations, as it has been found recently in first-principles calculations of  $BiFeO_3$ .<sup>41</sup> Figure 9(b) shows the enthalpies (in eV per 5-ion unit cell) calculated for different phases of PIN under pressure. All enthalpies are given with respect to  $P2_1/c$  phase, which in the initial state has  $Pbam$  symmetry. One can see that, according to this simulation, the  $Pbam$  ( $P2_1/c$ ) phase is the ground state until approximately 3 GPa, where  $R3$  phase proves to be slightly more stable. Above 5 GPa,  $Pnma$  (another  $P2_1/c$ ) phase becomes the ground state. Recall that all these data were calculated for the  $Fm-3m$  chemical configuration, which is for the NaCl structure. In contrast to this, the experiments were performed for disordered relaxor PIN. This disordered crystal may have a different phase diagram. Thus, from one point of view, if one changes the degree of order in PIN then the phase diagram can become richer. On the other hand, some phase transitions can fail, because of large energy barriers between the phases. For example,  $R3c$  group is not a subgroup or a parent group for  $Pbam$ . Thus, the phase transition between these two phases might require specific additional conditions. More experiments and first-principles analyses are necessary to understand the phase diagrams revealed in the present study.

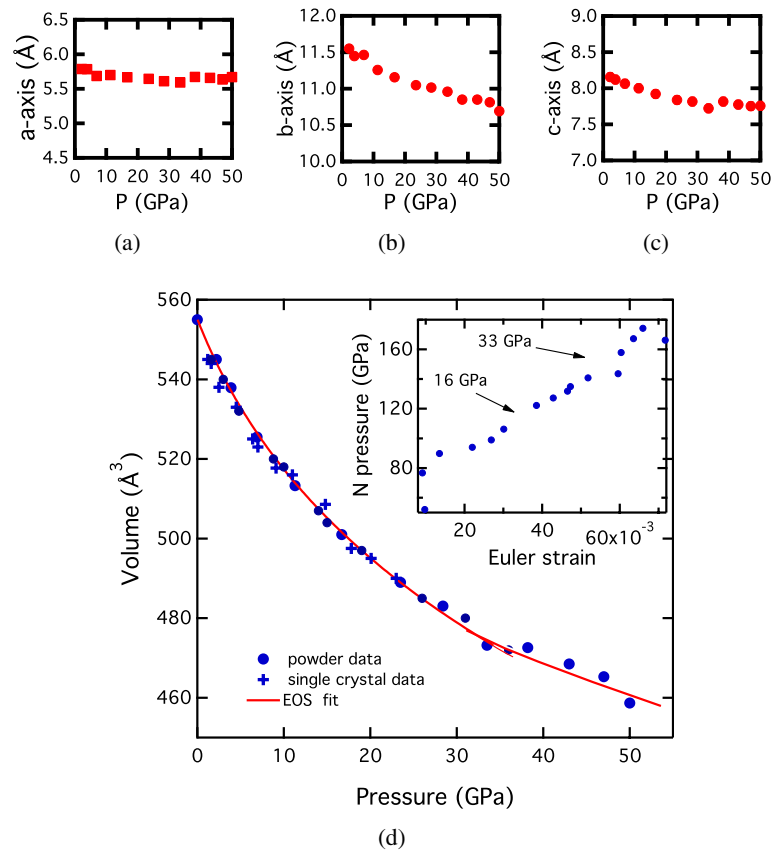


Fig. 7. Pressure dependencies of lattice parameters and unit cell volume. (a) *a*-axis, (b) *b*-axis, (c) *c*-axis, and (d) volume. Solid circles represent the unit cell volumes obtained from powder diffractions and crosses represent the single crystal data. Solid curve is a fit by third-order Birch–Murnaghan EOS, which yields a bulk modulus of  $79 (\pm 5)$  GPa, its pressure derivative of  $12 (\pm 4)$ , and an initial volume of  $560 (\pm 5) \text{ \AA}^3$ . Inset shows the normalized pressure (Eq. (1)) as the function of Euler strain (Eq. (2)).

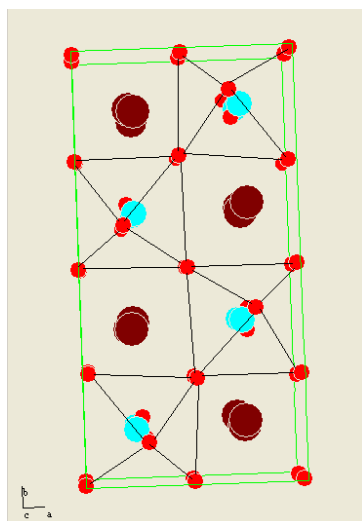


Fig. 8. Orthorhombic (*Pbam*) unit cell is shown for 3.9 GPa and obtained from our Rietveld refinement. Largest solid circles represent the Pb-cations, medium sized solid circle represent the In- or Nb-cations, and smallest solid circle represent the oxygen-anions. The figure shows Pb displacements in the  $\Sigma$ -mode (antiferroelectric displacements); and oxygen-octahedra rotations in the *R*-mode in Brillouin zone.

Table 1. The lattice parameters and unit cell volumes at selected pressures. The lattice parameters were obtained by Rietveld fitting up to 23.5 GPa, however, the Rietveld fitting did not work well above 28 GPa.

<i>P</i> (GPa)	<i>a</i> (Å)	<i>b</i> (Å)	<i>c</i> (Å)	$\beta$ (°)	<i>V</i> (Å <sup>3</sup> )
Orthorhombic (II)					
2.2	5.787(10)	11.549(27)	8.156(22)	90	545.0(5)
3.9	5.7851(11)	11.449(30)	8.122(22)	90	537.9(1)
6.9	5.686(2)	11.463(5)	8.063(5)	90	525.5(1)
11	5.699(18)	11.258(1)	8.001(25)	90	513.3(1)
Orthorhombic (II')					
17	5.668(15)	11.156(37)	7.921(27)	90	500.9(2)
24	5.644(16)	11.048(35)	7.838(23)	90	488.8(2)
28	5.61076	11.0143	7.81628	90	483.03
Monoclinic					
34	5.592(6)	10.959(1)	7.721(97)	91.1(5)	473.2(9)
38	5.671(5)	10.850(1)	7.816(27)	100.7(6)	472.6(1)
43	5.657(32)	10.850(1)	7.774(6)	100.5(5)	468.4(1)
47	5.634(46)	10.812(4)	7.751(23)	99.0(6)	465.2(7)
50	5.669(66)	10.691(2)	7.755(5)	102.0(7)	458.6(5)

Table 2. Rietveld fitting parameters at 3.9 bottom and 24 GPa. Note that the occupancy for In and Nb was not sensitive to the fitting; the Rietveld fitting did not work well above 28 GPa.

<i>P</i> (GPa)	3.9				24			
	<i>Pbam</i>				<i>Pbam</i>			
Symmetry	<i>x</i>	<i>y</i>	<i>z</i>	Uiso	<i>x</i>	<i>y</i>	<i>z</i>	Uiso
Atomic coordinate								
Pb1	0.747(5)	0.146(5)	0	0.048	0.735(5)	0.385(5)	0	0.015
Pb2	0.716(5)	0.126(5)	0.5	0.022	0.730(5)	0.130(6)	0.5	0.029
In3 (50%)	0.235(6)	0.124(5)	0.251(4)	0.088	0.244(4)	0.136(5)	0.25	0.072
Nb4 (50%)	0.235(6)	0.124(5)	0.251(4)	0.088	0.244(4)	0.136(4)	0.25	0.072
O5	0.292(5)	0.099(4)	0	0.086	0.282(5)	0.049(5)	0	0.013
O6	0.271(4)	0.152(4)	0.5	0.028	0.261(5)	0.135(5)	0.5	0.03
O7	0.025	0.260(5)	0.227(5)	0.086	0.025	0.266(6)	0.230(4)	0.017
O8	0	0.5	0.293(5)	0.02	0	0.5	0.282(5)	0.019
O9	0	0	0.273(5)	0.03	0	0	0.263(5)	0.066
Rp (%)	1.0				2.0			
Rwp (%)	1.4				3.5			
R(F <sup>2</sup> ) (%)	22				32			

#### 4. Discussion

Previous studies have shown that the dielectric properties of PIN depend strongly on heat treatment and synthesis conditions. A well-annealed PIN crystal shows chemical ordering in the arrangement of In<sup>3+</sup> and Nb<sup>5+</sup> on the B-site<sup>16</sup> and no frequency dispersions near the transition temperature. On the other hand, quenched PIN crystal shows disordering on the B-site with broad frequency dispersive dielectric permittivity.<sup>16</sup> Here we studied the disordered PIN samples and observed that the sequence of pressure-induced transitions in disordered PIN crystal are rather similar to that of PbZrO<sub>3</sub>.<sup>42</sup> The first transition occurs in disordered PIN at around 0.5 GPa, we observe strong diffuse scattering even at 1.2 GPa (Fig. 4) and it is believed that diffuse scattering strongly correlates to the polar nanoregions (PNRs) and relaxor behavior. Thus our result indicates that the PNRs may not affect the mechanism of pressure-induced transitions in PIN. It is generally accepted

the B-site chemical disorder and related local charge imbalance in Pb-based perovskites are the major factors for the occurrence of relaxor behavior.<sup>16,31,43</sup> In addition, the coexistence of competing forces of ferroelectric and anti-ferroelectric forces may play a certain role in the formation of the relaxor state.<sup>32,33,37,44–48</sup>

We observe two type of diffuse scatterings, one is along reciprocal lattice lines, and the other one is butterfly shaped around Bragg peak. We show that both type of diffuse scattering are suppressed by pressure. It has been shown that the butterfly shaped diffuse X-ray scattering is originated from PNRs in relaxors and is gradually suppressed with increasing pressure.<sup>21,22,24,37,49</sup> The Raman spectra obtained at high pressure in Pb-based relaxors is inconsistent with paraelectric cubic symmetry, and it also differs from the Raman spectra observed at low temperatures and ambient pressures. Several high-pressure studies on Pb-based relaxors such as PSN,<sup>20</sup> PMN,<sup>22</sup> PZT,<sup>23</sup> PZN-*x*PT,<sup>24</sup> PMN-*x*PT,<sup>7,35</sup> and PST,<sup>33</sup>

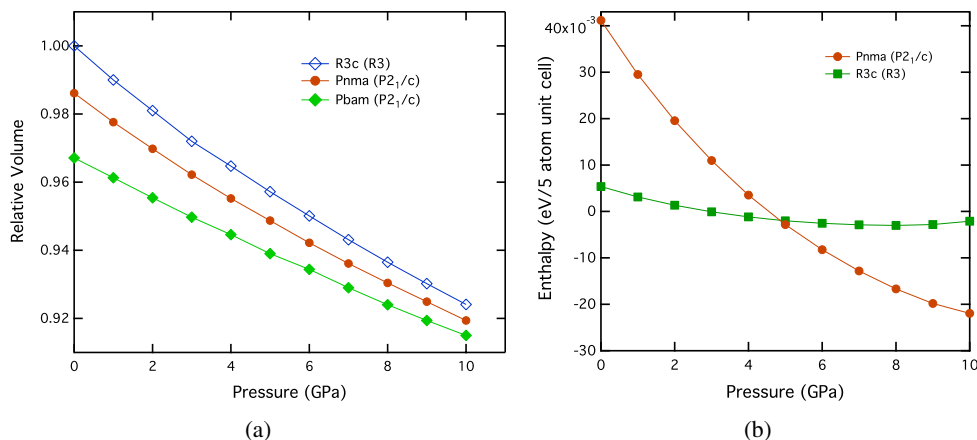


Fig. 9. (a) First-principles calculation of the pressure volume relations of the R3c (R3), Pbam (P<sub>21</sub>/c), and Pnma (P<sub>21</sub>/c) phases. (b) Pressure dependence of the relative enthalpy (in eV per 5 ion unit cell) for the Pbam (P<sub>21</sub>/c)-R3c (R3) and Pbam (P<sub>21</sub>/c)-Pnma (P<sub>21</sub>/c) phases.

suggested that the transition to the high-pressure phase involves octahedral tilting. These experimental findings indicate that pressure suppresses the ferroic atomic displacements existing at ambient conditions while favoring a long-range antiferrodistortive ordering. The difference with respect to the low temperature phases can be ascribed to the mechanism being similar but the structural subunits being distinct. In fact, our Rietveld refinement of the powder patterns (fitting example was shown in Fig. 6 (bottom) at 3.9 GPa) show that the isotropic thermal parameter,  $U$ , for Pb atom decreases with pressure from  $U_{\text{Pb}} = 0.048$  at 3.9 GPa to  $U_{\text{Pb}} = 0.015$  at 23 GPa.

Recent theoretical calculations and experiments point out that the displacement of Pb cation in these materials have strong correlations along particular crystallographic directions, that gives diffuse scattering in relaxor materials.<sup>37,49</sup> A common feature of high-pressure phase of Pb-based relaxors is a new peak appearing around  $380\text{ cm}^{-1}$  in Raman spectra for all these studied Pb-based relaxor samples including  $\text{PbTiO}_3$ . A similar peak appeared in PIN above 1 GPa, and the frequency of this peak is located around the bending mode region in general. Such a mode would appear from the distorted bending motion of oxygen due to tilting of octahedral units and their AFE displacements. At the same time, calculations<sup>50</sup> show that, above about 40 GPa, a ferroelectric like displacement of O might compete with the ferroelectric displacements of Nb or/and Pb, and this displacement might compete also with the tilting.

Our experiment is not definite about such ferroelectric like displacements and this can be also a consequence of the high potential barriers between the  $P_{\text{bam}}$  and  $R3c$  phases, preventing the appearance of the ferroelectric phase. Additionally, the random distribution of In over the lattice can also prevent the emergence of the  $R3c$  ferroelectric phase at high pressure. Indeed, it was shown<sup>51</sup> that the emergence of the ferroelectric phase at high-pressure stems from the interaction of d-transition-elements with oxygen ions, but In is not a d-element because its d-shell is fully occupied.

The coupling between PNRs and the soft-ferroelectric-mode also has been considered as a general feature of Pb-based perovskite relaxor ferroelectrics. For example, a highly damped soft mode was observed in PMN system by using neutron scattering,<sup>52</sup> and this behavior was attributed to the strong coupling between PNRs and the soft mode (the waterfall effect). In general, Samara *et al.*<sup>53</sup> suggested that the frequency of soft ferroelectric mode in ferroelectric materials is controlled by the delicate balance between long-range force and short-range force; and pressure can tune this balance and force the soft-mode to decrease its frequency with pressure. Alternatively, Kornev *et al.* proposed<sup>50</sup> that above about 40 GPa, oxygen bending can become ferroelectric. In relaxor ferroelectrics, additional forces can stem from the influence of pressure on the PNRs, by making PNRs to disappear with pressure. In particular, the emergence of the  $P_{\text{bam}}$  phase at low pressure can owe, in part, to this effect (at zero pressure,

the presence of PNRs can prevent the appearance of the homogeneous orthorhombic phase). Indeed, contrary to the ordered PIN, which has an antiferroelectric ground state with orthorhombic symmetry, the disordered PIN has a relaxor state with pseudo-cubic symmetry.

Thus, one can imagine that there exist more than two competing forces involved in the pressure induced successive transitions in the disordered PIN. They are soft mode (competition between ferroelectric long-range and short-range forces), octahedral tilting (the force which drives octahedral tilting), the PNRs. As observed, at the transition point between the relaxor and orthorhombic structures, happening for most Pb-based perovskite materials around 3–7 GPa, octahedral tilting overtakes the competition from the PNRs. After this transition, the enhanced octahedral tilting is the main force. We see this effect from the diminished diffuse scattering and the increased intensity of Raman peak around  $380\text{ cm}^{-1}$  with pressure. In spite of this fact, at higher pressure, another force enters the game and competes with the octahedral tilting, because at the second transition we observe clear splitting of the Bragg peak, around 16 GPa. At around 33 GPa, we observe further splitting of the Bragg peaks. This indicates that the orthorhombic symmetry is lowered in two steps. Such transitions are rather similar to ferroelastic transitions.<sup>54</sup> We believe that these transitions manifest a monoclinic distortion, which we also see in our first-principles calculations, but performed for the ordered PIN. At the same time, we cannot guarantee that the ground state of PIN at high pressure is nonpolar, because the bending displacements, in principle, can also lead to ferroelectricity,<sup>51</sup> while one should expect a first-order phase transition. But in our case, we have not detected the first-order jump. The fact that we have not detected it can be a consequence of the difficulty to overcome the large potential barriers (because of possible wide pressure hysteresis), or because of the random distribution of the nonferroelectric In over the lattice. The Raman line splitting can be also a consequence of increasing inhomogeneity of the lattice, under pressure, due to precursor phenomena.

## 5. Conclusions

A combination of Raman scattering, DFT calculations, and X-ray diffraction have been employed to investigate the behavior of PIN up to 50 GPa at 300 K. The structural transition from pseudo-cubic to orthorhombic at 0.5 GPa is associated with the appearance of a new peak at  $130\text{ cm}^{-1}$  and is consistent with the previous study. The transition at 16 GPa is accompanied by the splitting of the  $50\text{ cm}^{-1}$  peak above 16 GPa. We also observed a sharp peak near the  $380\text{ cm}^{-1}$  appears above 1 GPa and increases its intensity with pressure. The linewidth of the band at  $550\text{ cm}^{-1}$  also increases with pressure, and two of the Raman peaks merge toward 16 GPa. The third transition is observed at above 30 GPa. Raman spectra show drastic change below and above the transition.

The pressure evolution of the diffraction patterns for PIN shows obvious splitting above 30 GPa, particularly for pseudo-cubic [110] and [210] diffraction peaks; the results indicate a lowering symmetry transition in PIN. Our results indicate that PIN undergoes successive structural phase transitions under pressure. Changing balances between competing forces that result in octahedral tilting, long range ferroelectric ordering, and short range ordering is proposed to be the main mechanism for the transitions in PIN. The structure remains orthorhombic below and above 16 GPa through the transition, and is possibly the iso-structure transition due to the linear compressibility changes. The transition at 33 GPa is shown to be an orthorhombic to monoclinic transition. DFT calculations predict orthorhombic to monoclinic transitions under pressure, which is consistent with the experimental results.

### Acknowledgments

This work was sponsored by the Carnegie/Department of Energy Alliance Center (CDAC, DE-FC03-03NA00144). Use of the Advanced Photon Source was supported by the U. S. Department of Energy under Contract No. DE-AC02-06CH11357. HPCAT operations are supported by CIW, CDAC, UNLV, and LLNL through funding from DOE-NNSA and DOE-BES, with partial instrumentation funding by NSF. M. A. acknowledges ONR grants N00014-14-1-0561. S. P. acknowledges ONR grants N00014-12-1-1034. The computations were possible, thanks to the Arkansas High Performance Computer Center at University of Arkansas. S. P. also appreciates Russian Foundation for Basic Research Grant No. 14-02-90438\_Ucr\_a.

### References

- <sup>1</sup>S.-E. Park and T. R. Shrout, Ultrahigh strain and piezoelectric behavior in relaxor based ferroelectric single crystals, *J. Appl. Phys.* **82**, 1804 (1997).
- <sup>2</sup>D. Viehland, A. Amin and J. F. Li, Piezoelectric instability in 011-oriented  $\text{Pb}(\text{B}_{1/3}\text{B}_{2/3})\text{O}_3\text{-PbTiO}_3$  crystals, *Appl. Phys. Lett.* **79**, 1006 (2001).
- <sup>3</sup>P. K. Davies, Cation ordering in complex oxides, *Curr. Opin. Solid State Mater.* **4**, 467 (1999).
- <sup>4</sup>H. Fu and R. E. Cohen, Polarization rotation mechanism for ultrahigh electromechanical response in single-crystal piezoelectrics, *Nature* **403**, 281 (2000).
- <sup>5</sup>D. Vanderbilt and M. H. Cohen, Monoclinic and triclinic phases in higher-order Devonshire theory, *Phys. Rev. B* **63**, 094108 (2001).
- <sup>6</sup>B. Noheda, D. E. Cox, G. Shirane, J. Gao and Z.-G. Ye, Phase diagram of the ferroelectric relaxor  $(1-x)\text{PbMg}_{1/3}\text{Nb}_{2/3}\text{O}_3-x\text{PbTiO}_3$ , *Phys. Rev. B* **66**, 054104 (2002).
- <sup>7</sup>B. Chaabane, J. Kreisel, P. Bouvier, G. Lucazeau and B. Dkhil, Effect of high pressure on the  $\text{Pb.Mg}_{1/3}\text{Nb}_{2/3}\text{O}_3\text{-PbTiO}_3$  solid solution: A Raman scattering investigation, *Phys. Rev. B* **70**, 134114 (2004).
- <sup>8</sup>G. A. Samara, Relaxor properties of compositionally disordered perovskites: Ba- and Bi-substituted  $\text{Pb.Zr}_{1-x}\text{Ti}_x\text{O}_3$ , *Phys. Rev. B* **71**, 224108 (2005).
- <sup>9</sup>M. Ahart, M. Somayazulu, R. E. Cohen, P. Ganesh, P. Dera, H. K. Mao, R. J. Hemley, Y. Ren, P. Liermann and Z. Wu, Origin of morphotropic phase boundaries in ferroelectrics, *Nature* **451**, 545 (2008).
- <sup>10</sup>C. Malibert, B. Dkhil, J. M. Kiat, D. Durand, J. F. Berar and A. S. Bire, Order and disorder in the relaxor ferroelectric perovskite  $\text{PbSc}_{1/2}\text{Nb}_{1/2}\text{O}_3$  (PSN): Comparison with simple perovskites  $\text{BaTiO}_3$  and  $\text{PbTiO}_3$ , *J. Phys. Condens. Matter* **9**, 7485 (1997).
- <sup>11</sup>P. Groves, The influence of B-site cation order on the phase transition behaviour of antiferroelectric lead indium niobate, *J. Phys. C* **19**, 5103 (1986).
- <sup>12</sup>K. Nomura, T. Shingai, N. Yasuda, H. Ohwa and H. Terauchi, Phase transition in a relaxor  $\text{Pb}(\text{In}_{1/2}\text{Nb}_{1/2})\text{O}_3$ , *Ferroelectrics* **218**, 69 (1998).
- <sup>13</sup>K. Nomura, N. Yasuda, H. Ohwa and H. Terauchi, X-ray study of phase transitions in  $\text{PbIn}_{1/2}\text{Nb}_{1/2}\text{O}_3$ , *J. Phys. Soc. Jpn.* **66**, 1856 (1997).
- <sup>14</sup>N. Yasuda, H. Ohwa, J. Oohashi, K. Nomura, H. Terauchi, M. Iwata and Y. Ishibashi, Pressure-induced dielectric change from relaxor to antiferroelectric behavior in disordered  $\text{Pb}(\text{In}_{1/2}\text{Nb}_{1/2})\text{O}_3$ , *J. Phys. Soc. Jpn.* **66**, 1920 (1997).
- <sup>15</sup>K. Nomura, T. Shingai, N. Yasuda, H. Ohwa and H. Terauchi, Pressure-induced structural phase transition from relaxor phase to antiferroelectric phase in disordered  $\text{Pb}(\text{In}_{1/2}\text{Nb}_{1/2})\text{O}_3$ , *J. Phys. Soc. Jpn.* **68**, 866 (1999).
- <sup>16</sup>H. Ohwa, M. Iwata, H. Orihara, N. Yasuda and Y. Ishibashi, Observation of the distribution of the transition temperature in  $\text{Pb}(\text{In}_{1/2}\text{Nb}_{1/2})\text{O}_3$ , *J. Phys. Soc. Jpn.* **69**, 1533 (2000).
- <sup>17</sup>M. F. Kuprianov, A. V. Turik, S. M. Zaitsev and E. G. Fesenko, Phase transitions in  $\text{PbNb}_{0.5}\text{B}_{0.5}\text{O}_3$  (B = Sc, In), *Phase Transit.* **4**, 65 (1985).
- <sup>18</sup>A. A. Bokov, M. A. Leshchenko, M. A. Malitskaya and I. P. Raevski, Dielectric spectra and Vogel-Fulcher scaling in  $\text{Pb}(\text{In}_{0.5}\text{Nb}_{0.5})\text{O}_3$  relaxor ferroelectric, *J. Phys. Condens. Matter* **11**, 4899 (1999).
- <sup>19</sup>P. Groves, Phase transition behaviour in lead scandium tantalate, *Ferroelectrics* **76**, 81 (1987).
- <sup>20</sup>B. J. Maier, R. J. Angel, W. G. Marshall, B. Mihailova, C. Paulmann, J. M. Engel, M. Gospodinov, A.-M. Welsch, D. Petrovae and U. Bismayera, Octahedral tilting in Pb-based relaxor ferroelectrics at high pressure, *Acta Crystallogr. B* **66**, 280 (2010).
- <sup>21</sup>B. Chaabane, J. Kreisel, B. Dkhil, P. Bouvier and M. Mezouar, Pressure-induced suppression of the diffuse scattering in the model relaxor ferroelectric  $\text{PbMg}_{1/3}\text{Nb}_{2/3}\text{O}_3$ , *Phys. Rev. Lett.* **90**, 257601 (2003).
- <sup>22</sup>J. Kreisel, P. Bouvier, B. Dkhil, P. A. Thomas, M. A. Glazer, T. R. Welberry, B. Chaabane and M. Mezouar, High-pressure x-ray scattering of oxides with a nanoscale local structure: Application to  $\text{Na}_{1/2}\text{Bi}_{1/2}\text{TiO}_3$ , *Phys. Rev. B* **68**, 014113 (2003).
- <sup>23</sup>A. Sani, B. Noheda, I. A. Kornev, L. Bellaiche, P. Bouvier and J. Kreisel, High-pressure phases in highly piezoelectric  $\text{PbZr}_{0.52}\text{Ti}_{0.48}\text{O}_3$ , *Phys. Rev. B* **69**, 020105(R) (2004).
- <sup>24</sup>M. Ahart, R. E. Cohen, V. Struzhkin, E. Gregoryanz, D. Rytz, S. Prosandeev, H.-K. Mao and R. J. Hemley, High-pressure Raman scattering and x-ray diffraction of the relaxor ferroelectric  $0.96\text{Pb.Zn}_{1/3}\text{Nb}_{2/3}\text{O}_3\text{-}0.04\text{PbTiO}_3$ , *Phys. Rev. B* **71**, 144102 (2005).

- <sup>25</sup>M. Ahart, H.-K. Mao, R. E. Cohen, R. J. Hemley, G. A. Samara, Y.-H. Bing, Z.-G. Ye and S. Kojima, Pressure effects on relaxor ferroelectricity in disordered  $\text{Pb}(\text{Sc}_{1/2}\text{Nb}_{1/2})\text{O}_3$ , *J. Appl. Phys.* **107**, 074110 (2010).
- <sup>26</sup>M. Ahart, S. Kojima, N. Yasuda and R. J. Hemley, Successive pressure-induced structural transitions in relaxor lead indium niobate, *Ferroelectrics* **467**, 138 (2014).
- <sup>27</sup>Y. Feng, M. Somayazulu, R. Jaramillo, T. F. Rosenbaum, E. D. Isaacs, J. Hu and H.-K. Mao, Energy dispersive x-ray diffraction of charge density waves via chemical filtering, *Rev. Sci. Instrum.* **76**, 063913 (2005).
- <sup>28</sup>A. F. Goncharov and V. Struzhkin, Raman spectroscopy of metals, high-temperature superconductors and related materials under high pressure, *J. Raman Spectrosc.* **34**, 532 (2003).
- <sup>29</sup>J. P. Perdew, K. Burke and M. Ernzerhof, Generalized gradient approximation made simple, *Phys. Rev. Lett.* **77**, 3865 (1996).
- <sup>30</sup>G. Kresse and J. Furthmüller, Efficient iterative schemes for ab initio total-energy calculations using a plane-wave basis set, *Phys. Rev. B* **54**, 11169 (1996).
- <sup>31</sup>H. B. Krause, J. M. Cowley and J. Wheatley, Short-range ordering in  $\text{PbMg}_{1/3}\text{Nb}_{2/3}\text{O}_3$ , *Acta Crystallogr. A* **35**, 1015 (1979).
- <sup>32</sup>A.-M. Welsch, B. Mihailova, M. Gospodinov, R. Stosch, B. Guttler and U. Bismayer, High pressure Raman spectroscopic study on the relaxor ferroelectric  $\text{PbSc}_{0.5}\text{Nb}_{0.5}\text{O}_3$ , *J. Phys. Condens. Matter* **21**, 235901 (2009).
- <sup>33</sup>B. Mihailova, R. J. Angel, A.-M. Welsch, J. Zhao, J. Engel, C. Paulmann, M. Gospodinov, H. Ahsbahs, R. Stosch, B. Guttler and U. Bismayer, Pressure-induced phase transition in  $\text{PbSc}_{0.5}\text{Ta}_{0.5}\text{O}_3$  as a model Pb-based perovskite-type relaxor ferroelectric, *Phys. Rev. Lett.* **101**, 017602 (2008).
- <sup>34</sup>R. Shuker and R. W. Gammon, Raman-scattering selection-rule breaking and the density of states in amorphous materials, *Phys. Rev. Lett.* **25**, 222 (1970).
- <sup>35</sup>M. Ahart, S. Sinogeikin, O. Shebanova, D. Ikuta, Z.-G. Ye, H.-K. Mao, R. E. Cohen and R. J. Hemley, Pressure dependence of the monoclinic phase in  $(1-x)\text{Pb}(\text{Mg}_{1/3}\text{Nb}_{2/3})\text{O}_3-x\text{PbTiO}_3$  solid solutions, *Phys. Rev. B* **86**, 224111 (2012).
- <sup>36</sup>P. Dera, *Physics and Biophysics, High-Pressure Crystallography* (Springer, 2010).
- <sup>37</sup>P. Ganesh, E. Cockayne, M. Ahart, R. E. Cohen, B. Burton, R. J. Hemley, Y. Ren, W. Yang and Z.-G. Ye, Origin of diffuse scattering in relaxor ferroelectrics, *Phys. Rev. B* **81**, 144102 (2010).
- <sup>38</sup>P. R. Comes, M. Lambert and A. Guinier, Desordre lineaire dans les cristaux (cas du silicium, du quartz, et des perovskites ferroelectriques, *Acta Crystallogr. A* **26**, 244 (1970).
- <sup>39</sup>B. H. Toby, EXPGUI, a graphical user interface for GSAS, *J. Appl. Crystallogr.* **34**, 210 (2001).
- <sup>40</sup>R. Jeanloz, Shock wave equation of state and finite strain theory, *J. Geophys. Res.* **94**, 5873 (1989).
- <sup>41</sup>S. Prosandeev, D. Wang, W. Ren, J. Iniguez and L. Bellaich, Novel nanoscale twinned phases in perovskite oxides, *Adv. Funct. Mater.* **23**, 234 (2013).
- <sup>42</sup>Y. Kobayashi, S. Endo, L. C. Ming, K. Deguchi, T. Ashida and H. Fujishita, X-ray diffraction and dielectric measurements on  $\text{PbZrO}_3$  at high pressure: A phase transformation study, *J. Phys. Chem. Solids* **60**, 57 (1999).
- <sup>43</sup>B. P. Burton, E. Cockayne and U. V. Waghmare, Correlations between nanoscale chemical and polar order in relaxor ferroelectrics and the lengthscale for polar nanoregions, *Phys. Rev. B* **72**, 064113 (2005).
- <sup>44</sup>J. Kreisel, B. Dkhil, P. Bouvier and J. M. Kiat, Effect of high pressure on relaxor ferroelectrics, *Phys. Rev. B* **65**, 172101 (2002).
- <sup>45</sup>G. A. Samara, The relaxational properties of compositionally disordered  $\text{ABO}_3$  perovskites, *J. Phys. Condens. Matter* **15**, R367 (2003).
- <sup>46</sup>K. Z. Baba-Kishi, G. Cressey and R. J. Cernik, X-ray and electron diffraction studies of the structures of pseudo-perovskite compounds  $\text{Pb}_2(\text{Sc,Ta})\text{O}_6$  and  $\text{Pb}_2(\text{Mg,W})\text{O}_6$ , *J. Appl. Crystallogr.* **25**, 477 (1992).
- <sup>47</sup>N. Takesue, Y. Fujii, M. Ichihara and H. Chen, Self-accommodation of ionic size-effect atomic displacements in antiferroelectric order in relaxor lead scandium niobate, *Phys. Rev. Lett.* **82**, 3709 (1999).
- <sup>48</sup>R. J. Angel, J. Zhao and N. L. Ross, General rules for predicting phase transitions in perovskites due to octahedral tilting, *Phys. Rev. Lett.* **95**, 025503 (2005).
- <sup>49</sup>T. Yamanaka, M. Ahart, Y. Nakamoto, Z.-G. Ye, S. A. Gramsch, H.-K. Mao and R. J. Hemley, Anharmonic atomic vibrations in the relaxor ferroelectric  $\text{Pb}(\text{Mg}_{1/3}\text{Nb}_{2/3})\text{O}_3$  under pressure, *Phys. Rev. B* **86**, 174108 (2012).
- <sup>50</sup>I. A. Kornev, L. Bellaiche, P. Bouvier, P.-E. Janolin, B. Dkhil and J. Kreisel, Ferroelectricity of perovskites under pressure, *Phys. Rev. Lett.* **95**, 196804 (2005).
- <sup>51</sup>I. A. Kornev et al., The nature of ferroelectricity under pressure, *Phase Transit.* **80**, 385 (2007).
- <sup>52</sup>P. M. Gehring, S. Wakimoto, Z.-G. Ye and G. Shirane, Soft mode dynamics above and below the Burns temperature in the relaxor  $\text{Pb}(\text{Mg}_{1/3}\text{Nb}_{2/3})\text{O}_3$ , *Phys. Rev. Lett.* **87**, 277601 (2001).
- <sup>53</sup>G. A. Samara, T. Sakudo and K. Yoshimitsu, Important generalization concerning the role of competing forces in displacive phase transitions, *Phys. Rev. Lett.* **35**, 1767 (1975).
- <sup>54</sup>K. Aizu, General considerations of heterophase sequences of transitions, *J. Phys. Soc. Jpn.* **42**, 424 (1977).